# Crystallographic Characteristics of Delta-Ferrite Transformations in a 304L Weld Metal at Elevated Temperatures

*Ferrite shape and sigma precipitation at high temperatures are related to crystallographic ferrite structures*

BY H. KOKAWA, T. KUWANA AND A. YAMAMOTO

ABSTRACT. Delta-ferrite transformations and their crystallographic characteristics in a Type 304L austenitic stainless steel weld metal at elevated temperatures were observed mainly by transmission electron microscopy. Two types of ferrite morphologies, lacy and vermicular, coexist in the Type 304L steel weld metal. The lacy ferrite takes approximately the Kurdjumov-Sachs (K-S) relationship with austenite, but the vermicular one does not. Since the K-S relationship leads to a low-energy $\delta/\gamma$ boundary, the boundary coherency is higher in the lacy ferrite structure than in the vermicular one. These crystallographic characteristics are maintained in each ferrite structure during heat treatments. The two types of ferrite structures behaved quite differently in ferrite shape change and sigma precipitation on exposure to high temperatures. At 1073 K (1472°F), the ferrite shape tends to become rectangular and long-slender with a directionality in the lacy structure, while roundish in the vermicular one. Sigma precipitation at 973 K (1292°F) starts much earlier in the vermicular ferrite structure than in the lacy one. The larger the deviation angle of $\delta/\gamma$ from the K-S relationship, the easier is sigma precipitation. The large differences in transformation behavior between the two ferrite structures can be explained by $\delta/\gamma$ boundary coherency.

**KEY WORDS**

Crystallographic
Ferrite Shape
Sigma Precipitation
Delta-Ferrite
Austenitic Stainless
304L Stainless Steel
Lacy Ferrite
Vermicular Ferrite
Transformation Behavior
Kurdjumov-Sachs K-S

*H. KOKAWA and T. KUWANA are with the Department of Materials Processing, Tohoku University, Sendai, Japan. A. YAMAMOTO, former graduate student of Tohoku University, is with the Toshiba Corp.*

## Introduction

The presence of delta ferrite in austenitic stainless steel welds is known to avoid hot cracking during solidification (Refs. 1, 2). When the welds are exposed to elevated temperatures during service or postweld heat treatment, the delta ferrite changes in content and shape (Refs. 3, 4), and transforms into austenite, sigma or other phases (Refs. 5–11). Since the chemical compositions affect the changes and transformations, many discussions of previous studies are concentrated on local distributions of alloying or impurity elements (Refs. 4–13). On the other hand, these phenomena associated with phase transformations can also depend on the crystallographic characteristics of the structures, especially of ferrite-austenite interfaces as nucleation sites, but there seems to be very little knowledge about them.

Recently, it has been clarified that the ferrite morphology varies depending on the solidification mode (Refs. 14–21). The ferrite morphology is classified into several types, such as lathy, lacy, vermicular, etc. (Refs. 4, 14, 15). Transmission electron microscopic studies (Refs. 17, 18, 22, 23) have revealed that a lathy or lacy ferrite takes approximately the Kurdjumov-Sachs (K-S) orientation relationship (Ref. 24) with the austenite matrix, while a vermicular or eutectic ferrite does not. Such differences in crystallographic characteristics can affect subsequent phase transformations. In this study, the ferrite shape change and the sigma precipitation at elevated temperatures were investigated, from the viewpoint of crystallography, mainly by transmission electron microscopy (TEM) of a Type 304L weld metal, including several types of ferrite structures (Ref. 25).

## Experimental Procedure

Table 1 shows the chemical composition of the Type 304L stainless steel used in the present study. Stainless steel sheets of 150 × 45 × 10 mm (6 × 1.7 × 0.4 in.) in size, whose surfaces had been ground and cleaned to remove scale and dirt, were set in an atmosphere-controlled chamber (Ref. 23) under a traveling head of an automatic welding machine. The chamber was evacuated to a pressure of 10 Pa and then filled with argon gas at 0.1 MPa. The sheets were welded by the gas tungsten arc (GTA) process without filler metal in the chamber, eliminating the effects of gas absorption on the microstructure of the weld metal (Refs. 20, 23, 26). The welding conditions are shown in Table 2. The welded sheets were heat treated at 923 ~ 1073 K (1202° ~ 1472°F) for 0 ~ 1840 ks, and quenched in water. The specimens for observations and measurements were prepared from the heat-treated weld metals. The cross-section perpendicular to the welding direction was polished with emery papers and electrolytically etched in a 10% oxalic acid or a 10N KOH aqueous solution for optical microscope observations. The ferrite content was measured

**Table 1—The Chemical Composition of the Type 304L Stainless Steel Used in this Study (wt-%)**

| C | Si | Mn | P | S | Ni | Cr |
|---|---|---|---|---|---|---|
| 0.025 | 0.61 | 0.95 | 0.034 | 0.007 | 9.54 | 18.40 |

with a ferrite scope and a quantitative television microscope. Several slices about 1-mm (0.04-in.) thick were cut from each specimen parallel to the bead surface. The slices were electrolytically polished to about 0.3 mm (0.012 in.) in thickness, and disks 3 mm (0.12 in.) in diameter were cut from each slice by a spark machine. Thin-foil specimens were made from the disks by the jet-electropolishing technique in a 20% perchloric acid—80% acetic acid electrolytic solution. Each thin-foil specimen was observed under several diffraction conditions with a JEM-200B electron microscope operating at 200 kV. Much care was taken for location-to-location correspondence among these observations and measurements (Ref. 25). The crystallographic orientations were determined by electron diffraction patterns (Kikuchi lines and spot patterns). Particles of precipitate were identified by x-ray diffractometry of electrolytically extracted residue from heat-treated weld metals.

## Experimental Results and Discussions

### As-Welded Structure

Figure 1 shows the as-welded optical microstructure of the Type 304L steel. Two types of ferrite morphologies, lacy and vermicular (Ref. 4), coexist in the weld metal. Except for ferrite and austenite, no other phases were detected by x-ray diffractometry. Though the ferrite content varies depending on the location in the weld metal (Refs. 23, 25), the average value is about 10% in the central region of the weld metal. The local ferrite content is approximately 8% (about FN 9) in the vermicular ferrite area and is approximately 11% (about FN 13) in the lacy ferrite area. David reported that vermicular and lacy ferrite showed FN 9 ~ 12 and FN 13 ~ 15, respectively (Ref. 4). The weld metal obtained in the present study has a ferrite composition between vermicular and lacy, resulting in a mixed ferrite structure for them. The fraction of vermicular ferrite area is a little larger than that of the lacy one in the central area of this weld metal.

**Table 2—Welding Conditions**

| | |
|---|---|
| Polarity | Electrode negative |
| Electrode | W-1.7%Th (6-mm diameter) |
| Arc length | 10 mm |
| Welding current | 300 A |
| Arc voltage | 18 V |
| Travel speed | 10 cm/min (1.7 mm/s) |
| Welding atmosphere | argon, 0.1 MPa |

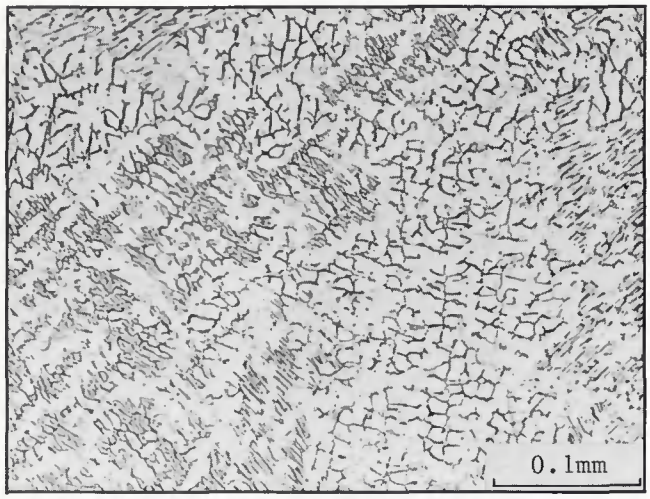


*Fig. 1—The optical microstructure in Type 304L weld metal*

Figure 2 shows an example of the TEM structure obtained from the lacy ferrite area in the as-welded specimen. The location-to-location correspondence between optical and transmission electron microstructures was confirmed by etching the thin foil which had been observed by TEM, *i.e.*, after TEM observation, the thin-foil specimen was electrolytically etched in a 10% oxalic acid aqueous solution, and the thinner region near the jet-polished perforation of the foil was observed by optical microscopy (Ref. 25). In order to examine crystallographic characteristics, the misorientation at the ferrite/austenite ($\delta/\gamma$) boundary was calculated in the following way (Ref. 23). The orientation relationship between the two neighboring phases is described by a rotation matrix (M) to transform orientations of the austenite phase into those of the adjacent ferrite phase. The experimental rotation matrix (M) of the $\delta/\gamma$ boundary misorientation in Fig. 2 is given by the Kikuchi lines.

$$M = \begin{pmatrix} -0.2296 & 0.9729 & -0.0277 \\ -0.6625 & -0.1354 & 0.7368 \\ 0.7130 & 0.1875 & 0.6756 \end{pmatrix} \quad (1)$$

Previous TEM studies (Refs. 18, 23) have shown that ferrite in structures resulting from single-phase ferritic solidification takes approximately the Kurdjumov-Sachs (K-S) orientation relationship (Ref. 24) with austenite. The K-S relation can lead to low-energy boundaries between ferrite and austenite. To evaluate the deviation from the exact K-S relationship, the deviation angle $\Delta\ \theta_{K\text{-}S}$ was used according to the recent special grain boundary study (Refs. 27–31). The $\Delta\ \theta_{K\text{-}S}$ is defined as follows: the misorientation (M) of a $\delta/\gamma$ boundary can be written by Equation 2

$$M = M_D\ M_{K\text{-}S} \quad (2)$$

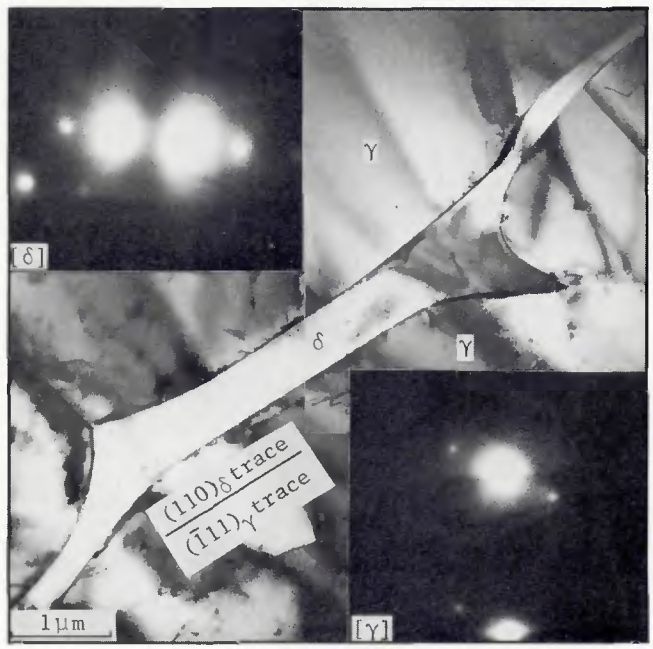


*Fig. 2—An example of the TEM structure obtained from the lacy ferrite area in the as-welded specimen. The Kikuchi line analyses of the electron diffraction patterns show that the incident electron beam direction is parallel to [1460 1552 9770] δ and [5603 3043 7704] γ*

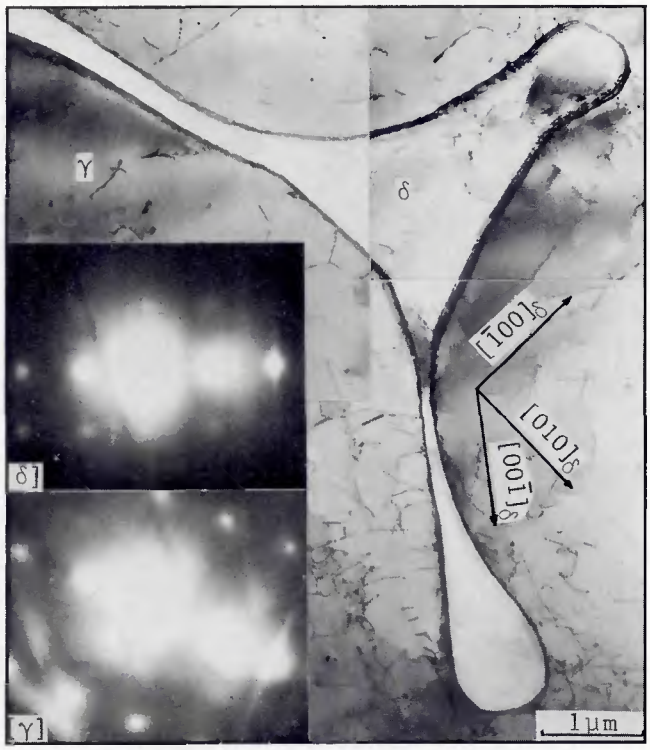


*Fig. 3—An example of the TEM structure obtained from the vermicular ferrite area in the as-welded specimen. The beam is parallel to [803 990 9918] δ and [128 297 1 9548] γ*

where $M_{K\text{-}S}$ and $M_D$ are the rotation matrices describing misorientation of the exact K-S relationship and deviation from the K-S relationship, respectively. The rotation angle of $M_D$ corresponds to the deviation angle $\Delta\,\theta_{K\text{-}S}$. (Since K-S relationship can be expressed by 576 equivalent transformation matrices, the smallest $\Delta\,\theta_{K\text{-}S}$ must be selected.) In the case of Fig. 2, $M_{K\text{-}S}$ and $M_D$ can be written by

$$M_{K\text{-}S} = \frac{1}{6}\begin{pmatrix} -1 & 1+2\sqrt{6} & -2+\sqrt{6} \\ 1-2\sqrt{6} & -1 & 2+\sqrt{6} \\ 2+\sqrt{6} & -2+\sqrt{6} & 4 \end{pmatrix} \quad (3)$$

$$M_D = \begin{pmatrix} 0.9927 & -0.0335 & -0.1158 \\ 0.0325 & 0.9995 & -0.0102 \\ 0.1161 & 0.0064 & 0.9932 \end{pmatrix} \quad (4)$$

The $\Delta\,\theta_{K\text{-}S}$ is calculated from $M_D$ to be 6.9 deg, which seems to be sufficiently small, and the orientation relationship between ferrite and austenite in Fig. 2 is near the K-S one. A K-S relationship makes a pair of parallel closed packed planes in ferrite and austenite. A major part of the $\delta/\gamma$ boundary is seen to be nearly parallel to the pair of planes ((110) $\delta$ // ($\bar{1}11$) $\gamma$). Such a boundary probably has high coherency.

Figure 3 shows an example of TEM structure obtained from the vermicular ferrite area in the as-welded specimen. Some branches of ferrite are elongated to <100> directions of ferrite, which are primary ferrite dendrite axes. The orientation relationship of the $\delta/\gamma$ is deviated largely from the K-S one ($\Delta\,\theta_{K\text{-}S}$ = 20.7 deg). This fact suggests that the $\delta/\gamma$ boundary has low coherency.

### Time-Temperature-Transformation Diagram

Figure 4 shows two examples of x-ray diffractometer results obtained from extracted heat-treated weld metals. Only $M_{23}C_6$ peaks were detected after a heat treatment at 1073 K for 350 ks (Fig. 4A), while sigma and $M_{23}C_6$ peaks were detected after a heat treatment at 973 K for 1300 ks—Fig. 4B. Chi and R phases, which are often observed in heat-treated Type 316 stainless steel metals (Refs. 5, 6, 8), were not detected in the heat-treated Type 304L stainless steel weld metals. Figure 5 shows the time-temperature-transformation (TTT) diagram given by the x-ray diffractometer results, together with the beginning lines of $M_{23}C_6$ and sigma precipitation in ferrite. The nose temperature (about 1000 K/1340°F) of the C-curve of sigma precipitation in the weld metal is higher than that (about 900 K/1160°F) of a solution-treated Type 304 steel, including no ferrite (Ref. 32). Figure 6 shows relations between the percent-ferrite remaining and the holding time at 973 K and 1073 K in the heat-treated weld metal. The percent-ferrite remaining is defined as the ratio of remaining ferrite content to the initial content in the as-welded structure (Ref. 9). As shown in Fig. 5, the delta-ferrite transforms to austenite and $M_{23}C_6$ at 1073 K, and to austenite, $M_{23}C_6$ and sigma at 973 K. The ferrite transformation at 973 K is slower in the early stage, but faster after being held a long time over 300 ks as compared to 1073 K. This fact may be attributed to sigma formation at 973 K.

### Microstructure Changes at 1073 K

In order to study shape instability of ferrite at high temperatures, the heat-treated weld metals at 1073 K, accompanied by no sigma precipitation, were observed. Figure 7 shows optical microstructural changes at 1073 K in two typical ferrite morphologies in the weld metal, *i.e.*, lacy and vermicular structures—Fig. 1. The series of optical microstructur-

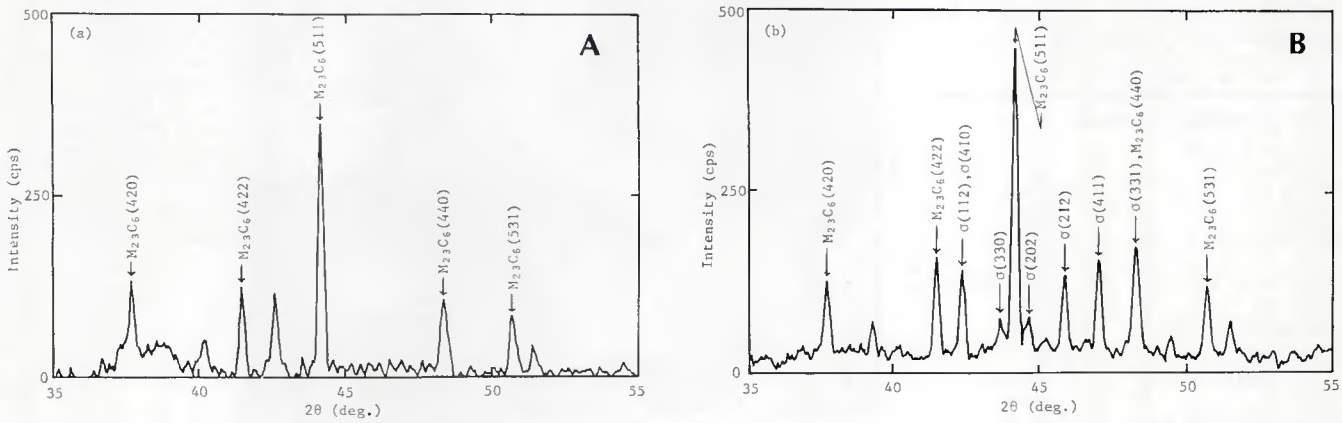


*Fig. 4—Examples of x-ray diffractometer results from extracted heat-treated weld metals. A—At 1073 K for 350 ks; B—at 973 K for 1300 ks*

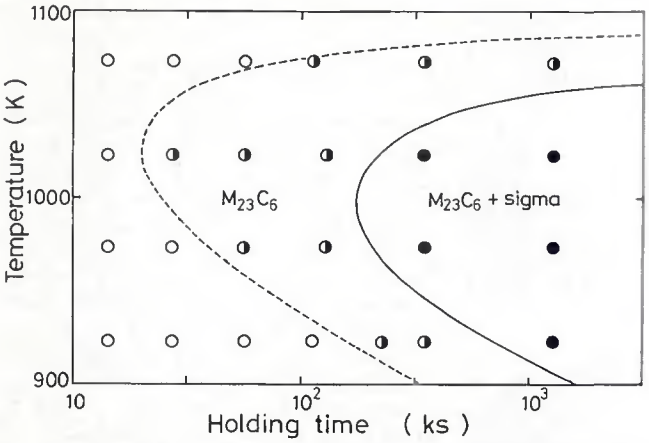


*Fig. 5 — The time-temperature-transformation diagram as determined by x-ray diffractometer results and optical microscope observations, shown together with beginning lines of $M_{23}C_6$ and the sigma precipitation in ferrite. Open circles indicate no precipitations were detected. Half-solid circles indicate $M_{23}C_6$ precipitation, and solid circles indicate both sigma and $M_{23}C_6$ precipitations*

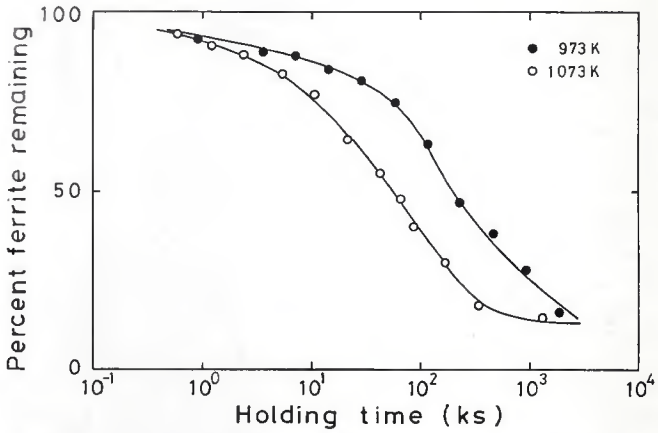


*Fig. 6 — Relations between the percent-ferrite remaining and the holding time at 973 K and 1073 K*

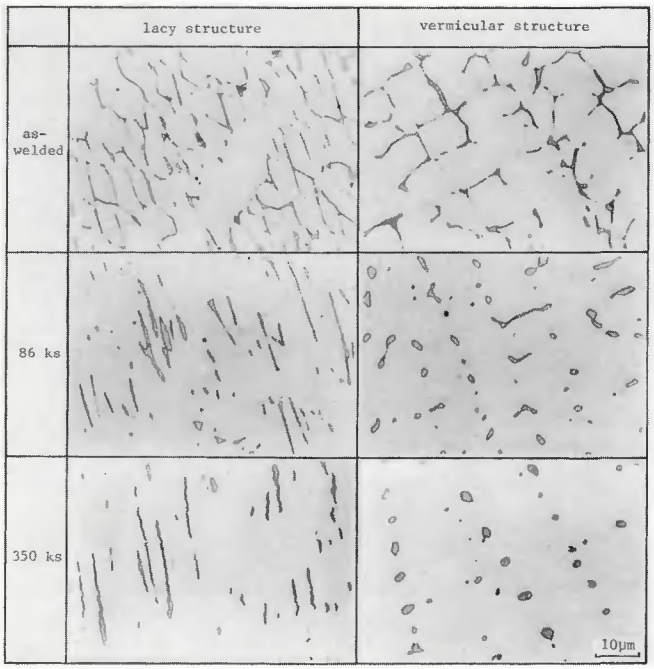


*Fig. 7 — Optical microstructural changes at 1073 K in lacy and vermicular structures*

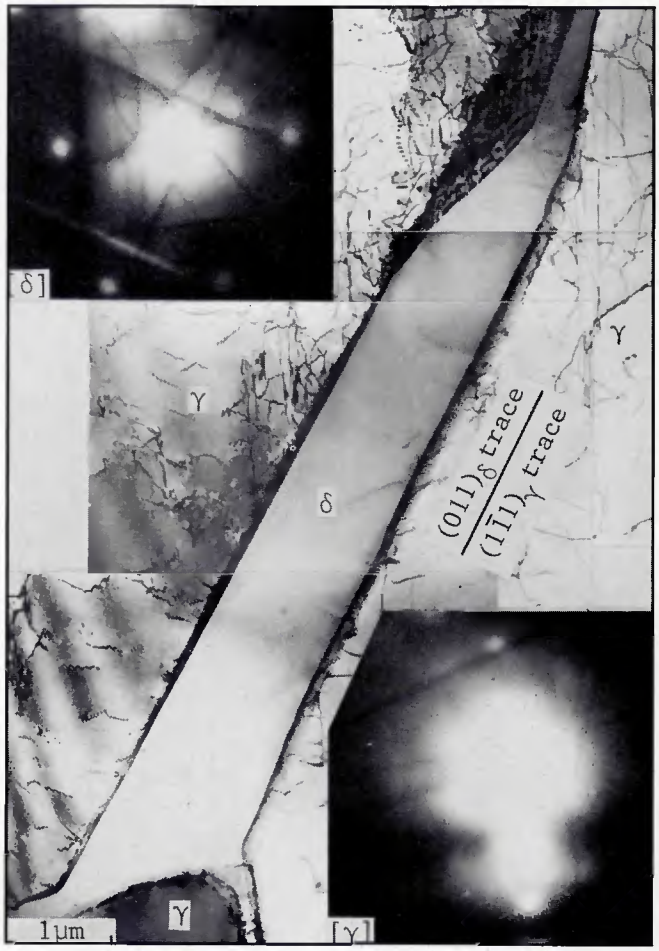


*Fig. 8 — An example of the TEM structure obtained from the lacy ferrite area in weld metal heat treated at 1073 K for 86 ks. The beam is parallel to [5390 2303 8102] δ and [6258 1208 7706] γ*

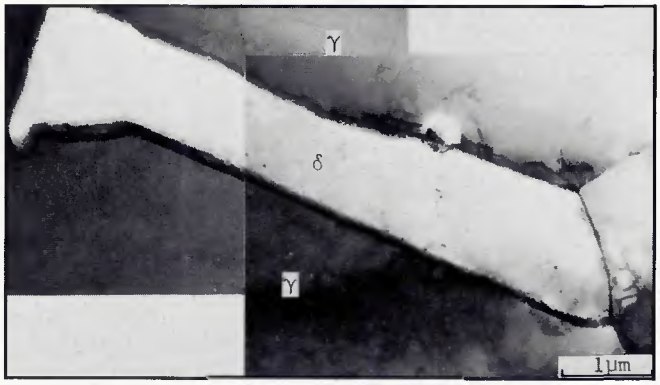


*Fig. 9 — An example of the TEM structure obtained from the lacy ferrite area in weld metal heat treated at 1073 K for 350 ks*

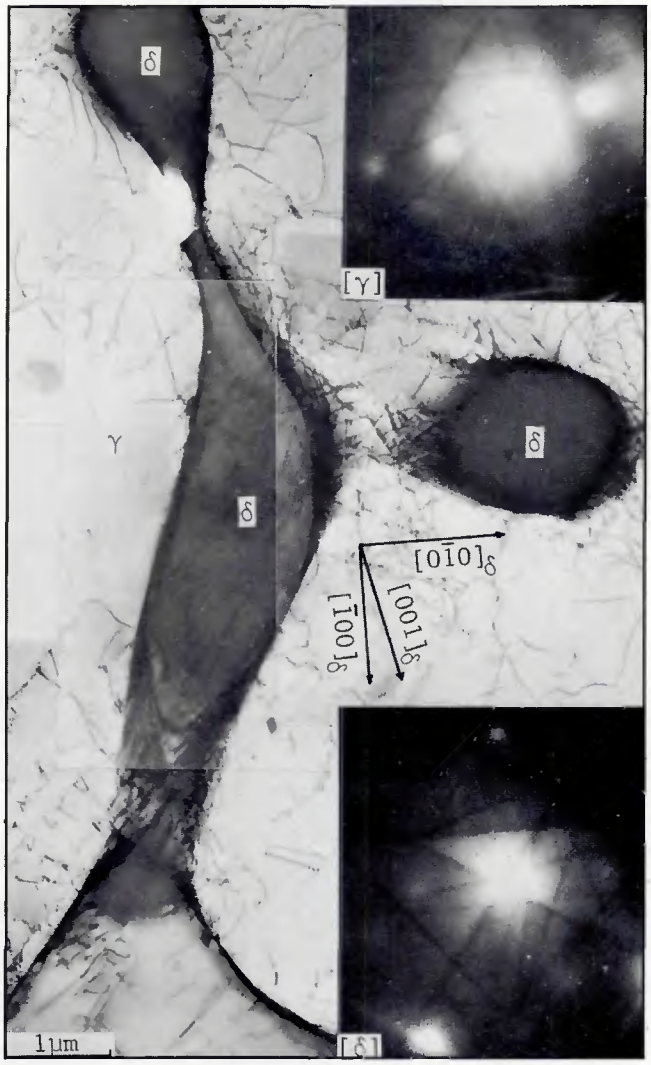


*Fig. 10—An example of the TEM structure obtained from the vermicular ferrite area in weld metal heat treated at 1073 K for 86 ks. The beam is parallel to [3392 667 9383] δ and [174 5021 8646] γ*

es were taken from almost the same locations in a specimen. In both structures, the fraction of ferrite-phase diminishes with the holding time and the ferrite networks are broken down. A long-time heat treatment changes the ferrite shape, depending on the initial ferrite structure. After 350 ks, the ferrite is long-slender with a directionality in the lacy structure, but is roundish in the vermicular one. The difference can be explained by their crystallographic characteristics as discussed later.

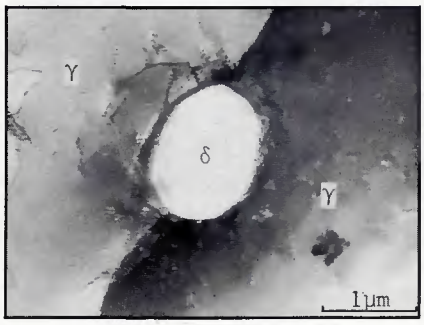


*Fig. 11—An example of the TEM structure obtained from the vermicular ferrite area in weld metal heat treated at 1073 K for 350 ks*

Figure 8 shows an example of the TEM structure obtained from the lacy ferrite area in the weld metal heat treated at 1073 K for 86 ks. The ferrite shape is rather rectangular and faceted. The $\delta/\gamma$ takes a near K-S relationship ($\Delta\ \theta_{K\text{-}S}$ = 8.7 deg), and the long-straight part of the boundary is nearly parallel to the pair of planes ( (011) $\delta$ // ($\bar{1}\bar{1}1$) $\gamma$). Even after 350 ks at 1073 K, these characteristics (taking a near K-S relationship and faceting) seem to remain in the lacy ferrite area, as in Fig. 9 ($\Delta\ \theta_{K\text{-}S}$ = 6.4 deg).

On the other hand, the vermicular ferrite is dissolved with necking at 1073 K, as shown in Fig. 10 (after 86 ks, $\Delta\ \theta_{K\text{-}S}$ = 31.5 deg), and breaks down into small roundish parts as shown in Fig. 11 (after 350 ks, $\Delta\ \theta_{K\text{-}S}$ = 29.2 deg).

The difference in crystallographic characteristics between the two ferrite structures may be related to whether the second phase nucleates in the liquid or solid phase. Nucleation in the solid phase may have a strong tendency to make a low energy boundary, such as the K-S relationship, while nucleation in the liquid may not. The lacy and vermicular ferrite structures probably result from the former and latter cases in the Type 304L steel weld, respectively. The difference in boundary energy affects ferrite shape changes in the two types of ferrite structures, *i.e.*, vermicular ferrite having high boundary energy becomes roundish to minimize the boundary plane, while lacy ferrite having low boundary energy becomes rectangular with some habit planes. The results of judgments by ferrite shape, to be rectangular or roundish, suggest that the critical value of $\Delta\ \theta_{K\text{-}S}$ between lacy and vermicular is about 12 deg in the present observations.

#### Microstructure Changes at 973 K

Figure 12 shows optical microstructural changes in the two typcial ferrite morphologies (lacy and vermicular) in the weld metal at 973 K. After 230 ks, sigma precipitation occurs in some of the vermicular ferrite grains, but does not in the lacy ones. After 1840 ks, all of the vermicular ferrite grains are fully covered with sigma, while a lot of lacy ferrite grains still remain without sigma. The sigma precipitation is suggested to start much earlier in vermicular ferrite than in the lacy one. Optical observations showed that the holding time at 973 K for sigma precipitation to start was 115 ks in the vermicular ferrite and 460 ks in the lacy one. This fact may be related to their crystallographic characteristics. (The optical observation already indicated a few sigma phases in vermicular ferrite grains slightly before the sigma start-line in the TTT diagram in Fig. 5. It may be because the amount of sigma was not enough for x-ray diffractometry to detect.)

In the TEM structures of weld metal heat treated at 973 K for 350 ks, a lot of ferrite grains were sigma-free, but a few had partially transformed to sigma, as shown in Fig. 13. Since the orientation relationship of the $\delta/\gamma$ deviated largely from the K-S one ($\Delta\ \theta_{K\text{-}S}$ = 34.2 deg), the ferrite may be vermicular. The sigma takes approximately the Nenno orientation relationship (Refs. 33, 34) with the austenite, but no low-index orientation relationship with the ferrite. The Nenno relationship is written by

$$(111)\ \gamma\ //\ (001)\ \sigma,\ [\bar{1}01]\ \gamma\ //\ [110]\ \sigma \quad (5)$$

The Nenno orientation relationship is known to lead to a low-energy $\sigma/\gamma$ boundary (Refs. 33–39). The orientation relationship between the sigma and austenite in Fig. 13 is stereographically projected in Fig. 14. The deviation angle from the Nenno relationship ($\Delta\ \theta_N$) is given as 3.4 deg with a similar calculation in the case of the K-S one. In the weld metal heat treated at 973 K for 350 ks, some sigma grains were isolated in the

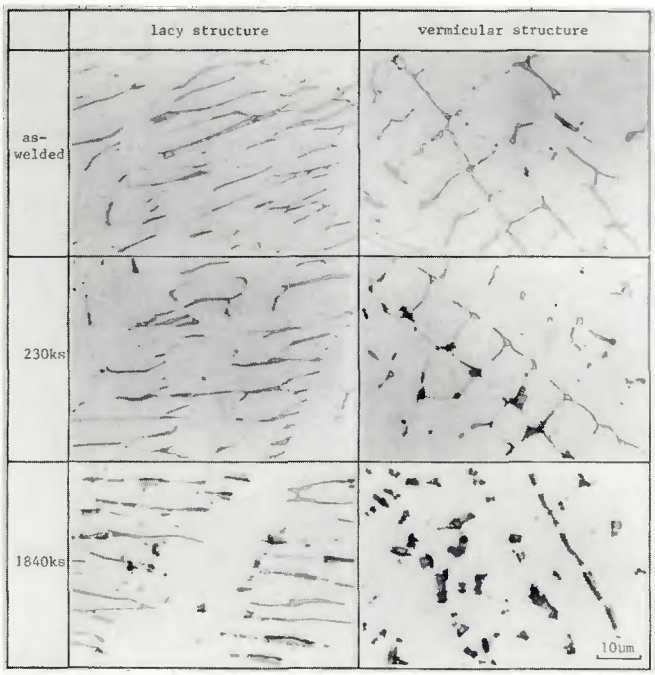


*Fig. 12 — Optical microstructural changes at 973 K in lacy and vermicular structures*

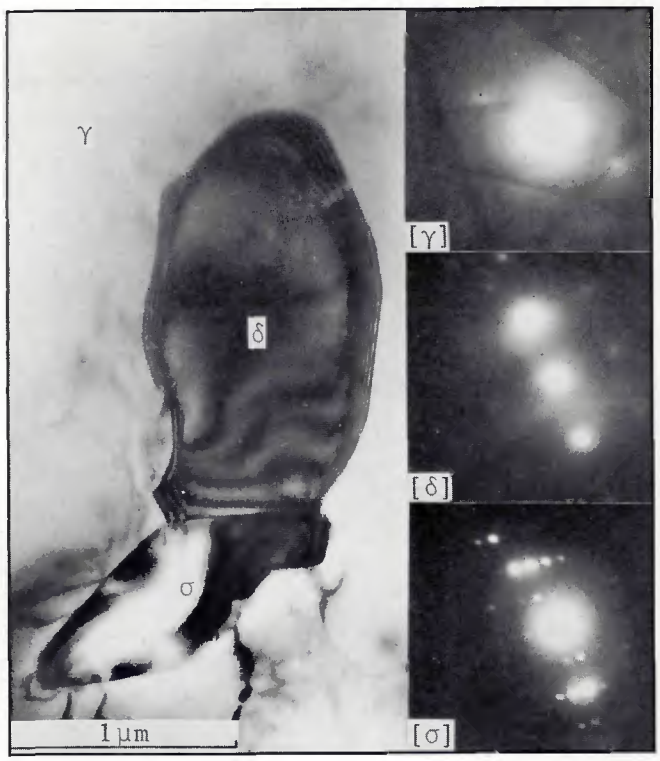


*Fig. 13 — An example of TEM structure obtained from the vermicular ferrite area in weld metal heat treated at 973 K for 350 ks. The beam is parallel to [649 738 9952] δ, [687 2178 9736] γ and [0$\bar{1}$1] σ*

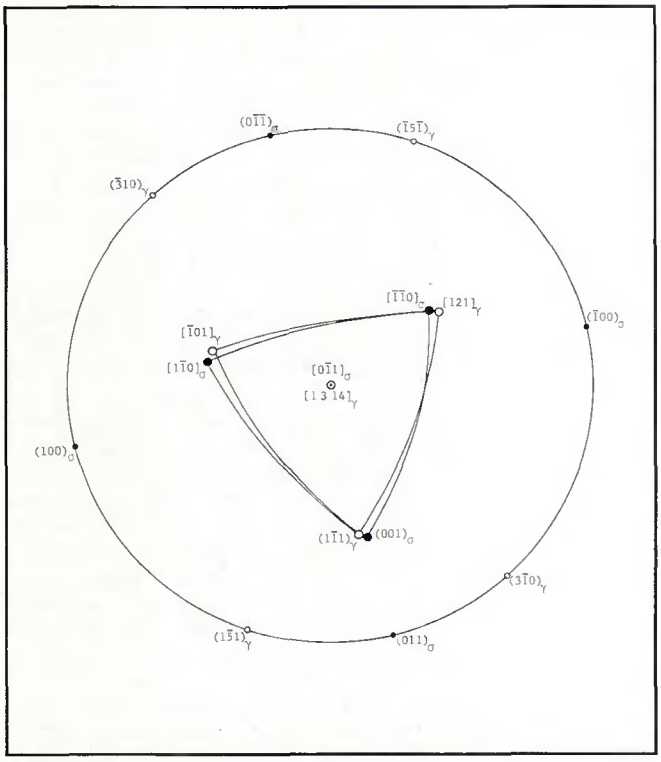


*Fig. 14 — The stereographic projections of the sigma and the austenite in Fig. 13*

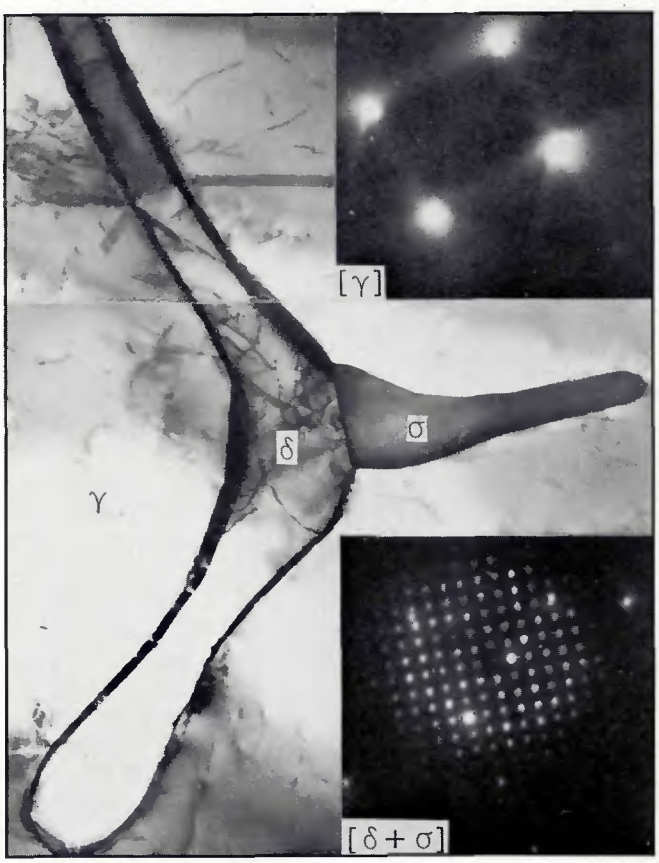


*Fig. 15 — An example of the TEM structure obtained from the vermicular ferrite area in weld metal heat treated at 973 K for 670 ks. The beam is parallel to [111] δ, [323] γ and [001] σ*

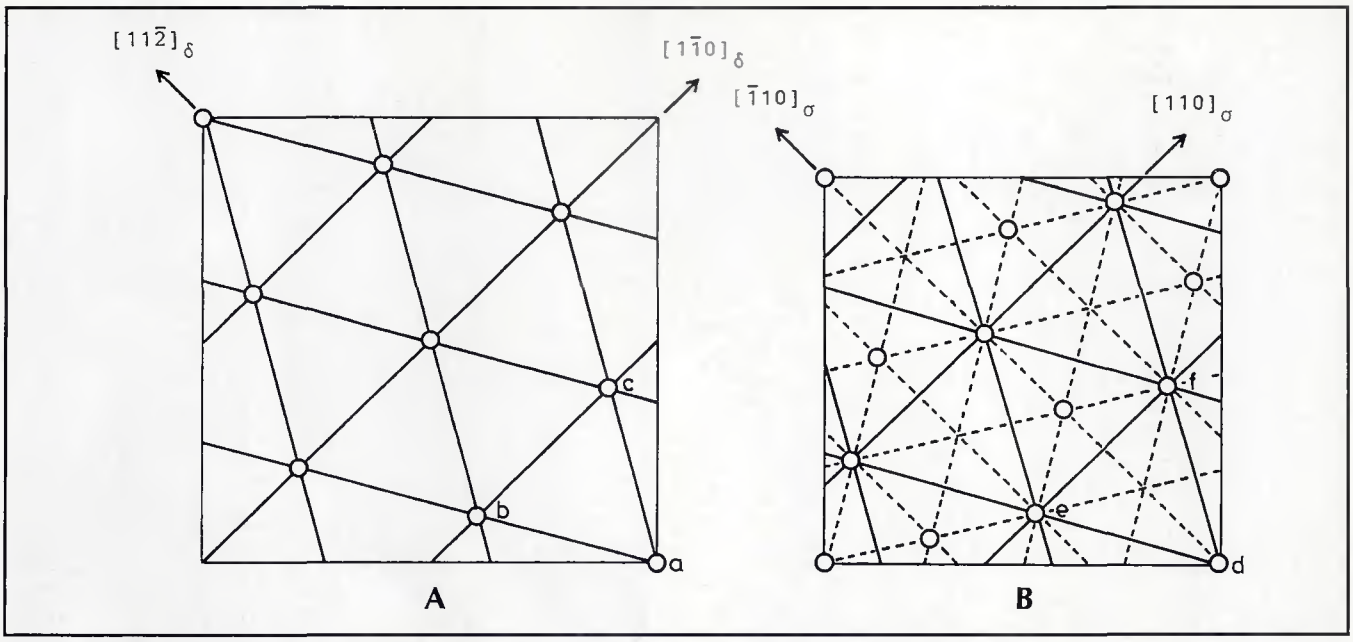


*Fig. 16—Atomic configurations of (111) δ and (001) σ planes, A and B respectively, in the relationship of Equation 6*

austenite matrix, and the others were observed only at the $\delta/\gamma$ boundaries of vermicular ferrite grains (having large $\Delta\ \theta_{K\text{-}S}$) and tend to take the Nenno relationship with austenite. No sigma was observed at the $\delta/\gamma$ boundaries of the lacy ferrite grains (having a small $\Delta\ \theta_{K\text{-}S}$).

In the weld metal heat treated at 973 K for 670 ks, several types of sigma precipitations were observed in addition to the type shown in Fig. 13. Figure 15 is an example of vermicular ferrite ($\Delta\ \theta_{K\text{-}S}$ = 29.8 deg) partially transformed to sigma. Though the relationship between the sigma and austenite deviates somewhat from the Nenno relationship ($\Delta\ \theta_N$ = 10.2 deg), the sigma takes the relationship with the ferrite of Equation 6 below, as shown by the diffraction patterns in Fig. 15 (the deviation angle $\Delta\ \theta_6$ from the relationship with Equation 6 is nearly 0 deg).

$$(111)\ \delta\ //\ (001)\ \sigma,\ [1\bar{1}0]\ \delta\ //\ [110]\ \sigma \quad (6)$$

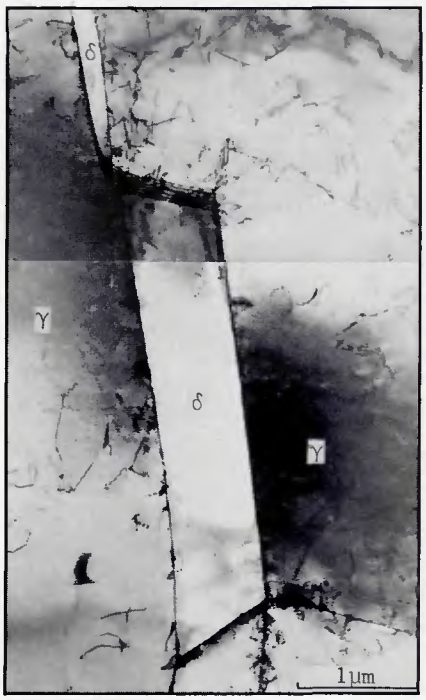


*Fig. 17—An example of the TEM structure obtained from the lacy ferrite area in the weld metal heat treated at 973 K for 670 ks*

The relationship with Equation 6 is derived by replacing orientations of austenite in the Nenno relationship with those of ferrite. Figure 16 shows atomic configurations of (111) $\delta$ and (001) $\sigma$ planes in the relationship. Since the triangles a-b-c and e-f-g are quite similar to each other, the relationship may lead to a low-energy $\delta/\gamma$ boundary. In the weld metal heat treated at 973 K for 670 ks, most of the ferrite grains partially transformed to sigma were vermicular, and all the sigma-free ferrite grains were lacy as shown in Fig. 17. Only a few lacy ferrite phases had transformed partially to sigma. Three examples of them are shown in Figs. 18–20. A lacy ferrite ($\Delta\ \theta_{K\text{-}S}$ = 8.7 deg) partially transformed to a sigma is shown in Fig. 18. The sigma does not take the Nenno relationship with the austenite ($\Delta\ \theta_N$ = 33.3 deg), but takes approximately the relationship of Equation 6 with the ferrite ($\Delta\ \theta_6$ = 7.4 deg). In Fig. 19, a lacy ferrite ($\Delta\ \theta_{K\text{-}S}$ = 4.2 deg) has two sigma grains whose crystallographic orientations are almost parallel to each other. The sigma grains take approximately the Nenno relationship ($\Delta\ \theta_N$ = 0.9 deg). The electron diffraction analysis of Fig. 19 reveals that the highest coherency between $\delta$ and $\gamma$ occurs on the planes $(10\bar{1})\ \delta\ //\ (11\bar{1})\ \gamma$, while the highest coherency between $\gamma$ and $\sigma$ occurs on the planes $(1\bar{1}1)\ \gamma\ //\ (001)\ \sigma$, *i.e.*, the $\{111\}\ \gamma$ planes are not the same. This suggests sigma precipitation on the coherent planes is very difficult. Figure 20 shows another example of lacy ferrite ($\Delta\ \theta_{K\text{-}S}$ = 5.4 deg) having two sigma grains. Though crystallographic orientations of the two sigma grains are not parallel to each other, each of them takes approximately the Nenno relationship with the austenite ($\Delta\ \theta_N$ = 0.9 deg in both cases), *i.e.*, $(11\bar{1})\ \gamma\ //\ (001)\ \sigma_1\ //\ (001)\ \sigma_2$, $[101]\ \gamma\ //\ [\bar{1}10]\ \sigma_1$, $[011]\ \gamma\ //\ [\bar{1}10]\ \sigma_2$.

Figure 21 shows the effects of the deviation angle from the K-S relationship on sigma precipitation at $\delta/\gamma$ boundaries in weld metals heat treated at 973 K for 350 ks and 670 ks, together with the frequency of the Nenno and Equation 6 relationships. The $\delta/\gamma$ boundary coherency decreases by increasing the deviation angle from the K-S relationship. In the early stage of the heat treatment (350 ks), sigma precipitation tends to be concentrated within the large deviation angle region. This fact suggests that the lower the $\delta/\gamma$ boundary coherency, the easier is sigma precipitation. Since $\delta/\gamma$ boundary coherency is high in lacy ferrite and low in the vermicular type, sigma precipitation may start earlier in vermicular ferrite. After heat treatment for 670 ks, such a tendency is weakened. This means that a heat treatment for a long time results in sigma precipitation even at highly coherent $\delta/\gamma$ boundaries. In the weld metal heat treated for 670 ks, sigma-free ferrite grains and isolated sigma phases (not contacted with ferrite) were observed. All of the sigma-free ferrite grains are lacy

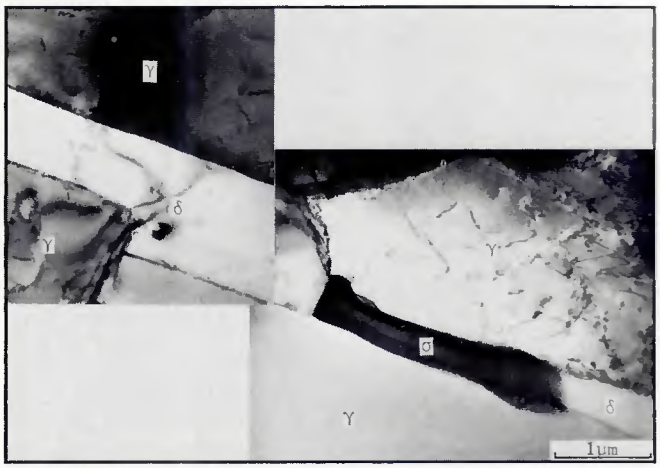


*Fig. 18 — An example of the TEM structure obtained from the lacy ferrite area in weld metal heat treated at 973 K for 670 ks*

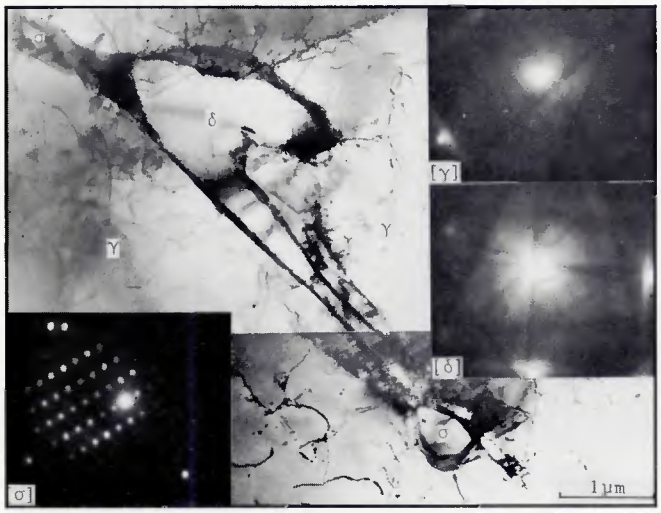


*Fig. 19 — An example of the TEM structure obtained from the lacy ferrite area in weld metal heat treated at 973 K for 670 ks. The beam is parallel to [6172 1730 7676] δ, [2081 4784 8531] γ and [1$\bar{1}\bar{1}$] σ*

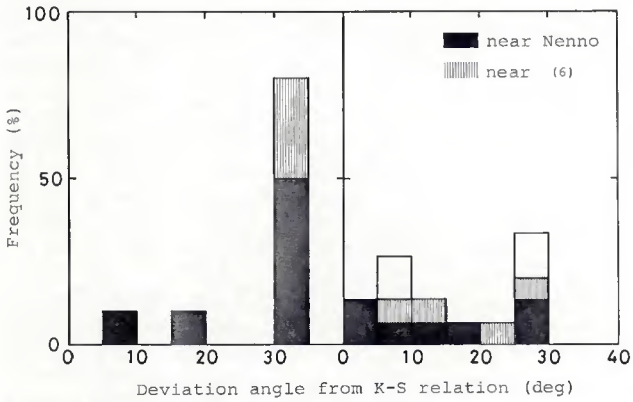


*Fig. 21 — Effects of the deviation angle from the K-S relationship on the sigma precipitation at δ/γ boundaries in specimens heat treated at 973 K for 350 ks and 670 ks, together with the frequency of γ/σ and δ/σ relationships (Nenno and Equation 6 relationships)*

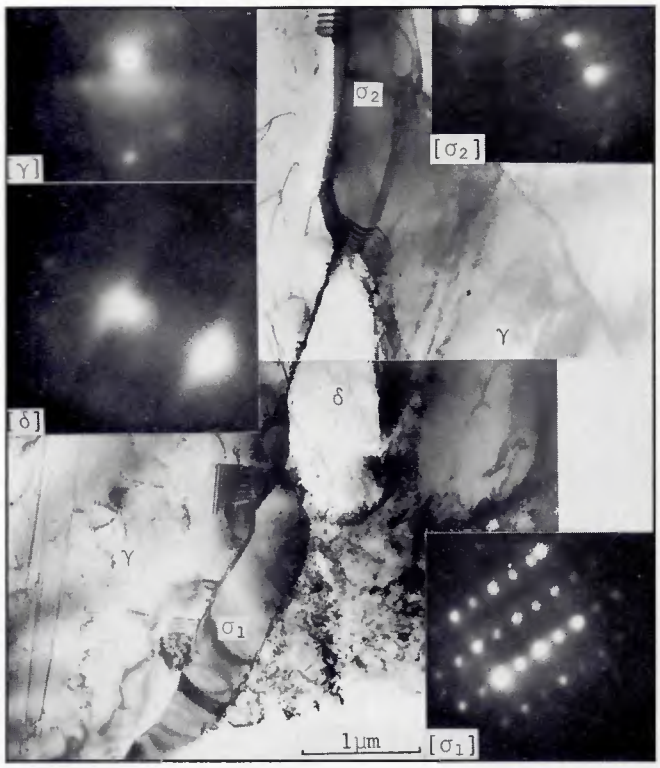


*Fig. 20 — An example of TEM structure from the lacy ferrite area in weld metal heat treated at 973 K for 670 ks. The beam is parallel to [5714 1099 8133] δ, [4949 4279 7563] γ, [$\bar{1}$30] $\sigma_1$ and [$\bar{1}3\bar{1}$] $\sigma_2$*

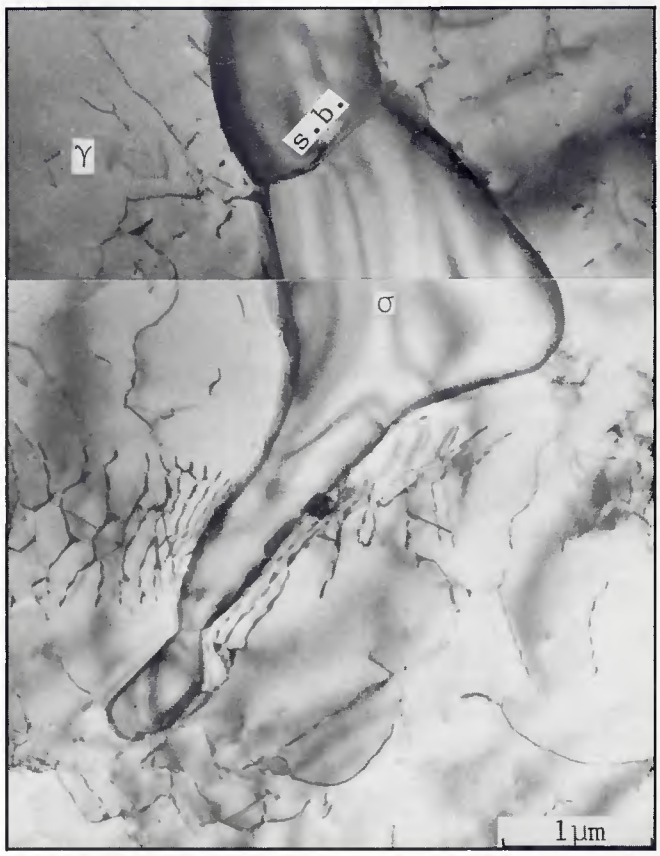


*Fig. 22 — An example of the TEM structure in weld metal heat treated at 973 K for 1300 ks*

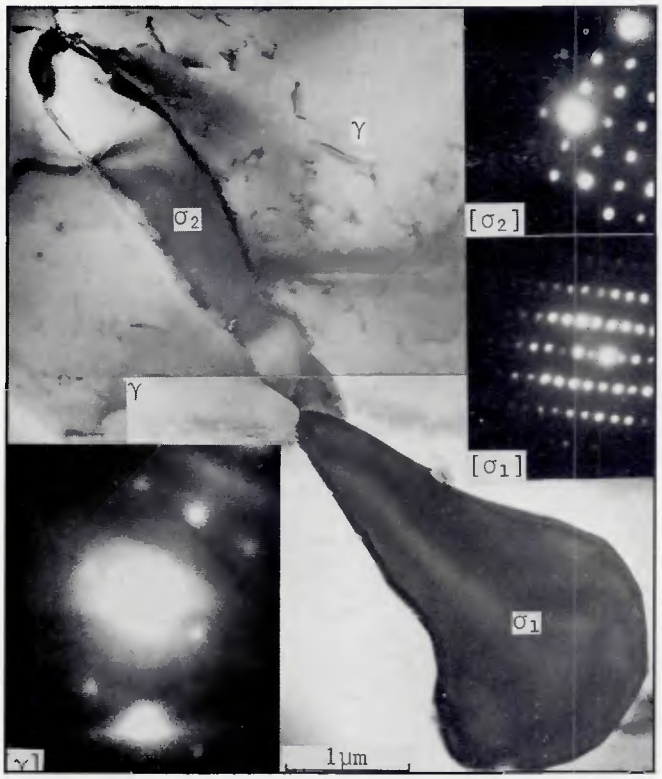


*Fig. 23 — An example of the TEM structure in weld metal heat treated at 973 K for 1300 ks. The beam is parallel to [33 35 60] γ, [01$\bar{1}$] $\sigma_1$ and [2$\bar{1}$2] $\sigma_2$*

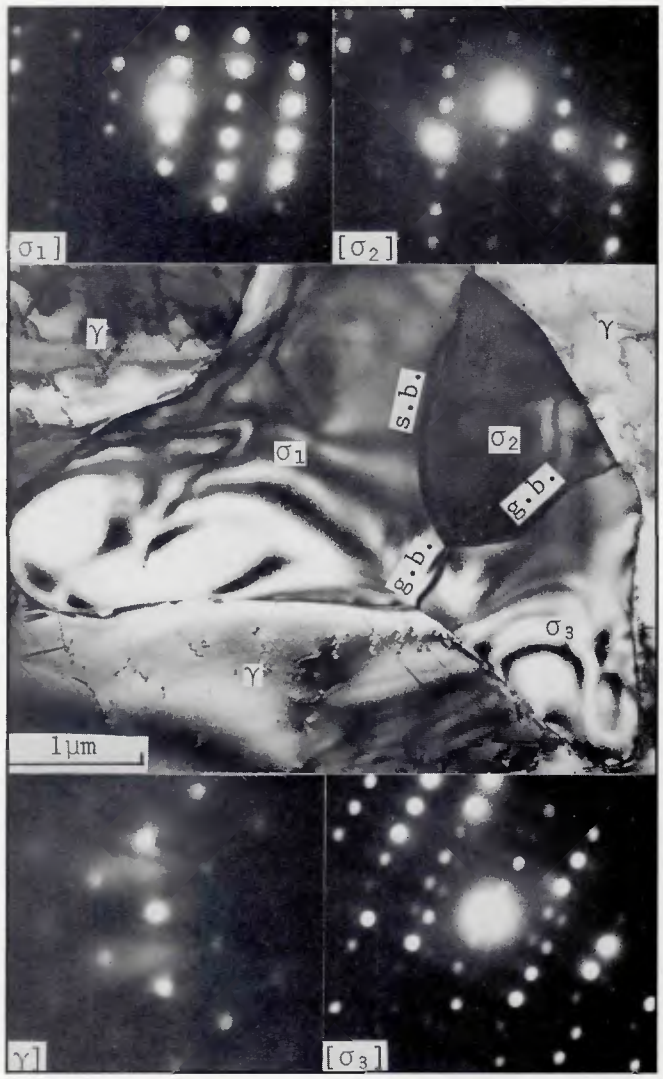


*Fig. 24 — An example of the TEM structure in weld metal heat treated at 973 K for 1300 ks. The beam is parallel to [111] γ, [1$\bar{4}$1] $\sigma_1$, [1$\bar{4}$1] $\sigma_2$ and [$\bar{1}$30] $\sigma_3$*

ones with a high coherency as shown in Fig. 17. Many of the isolated sigma phases may have resulted from the full transformation of vermicular ferrite. These results are consistent with optical microstructural changes shown in Fig. 12, *i.e.*, sigma precipitation is easier in vermicular ferrite than in the lacy one because of the $\delta/\gamma$ boundary coherency. Figure 21 also shows that most of sigma grains take the Nenno relationship with austenite or the Equation 6 relationship with ferrite.

In the weld metal heat treated at 973 K for a long time (1300 ks) ferrite phases were seldom observed, but small isolated sigma phases were often observed. Many of the sigma phases take approximately the Nenno relationship with austenite, but some of them do not. The sigma phases often include grain boundaries, as shown in Figs. 22–24. Many of them are subboundaries (small angle boundaries), as seen in Fig. 22 ($\Delta\,\theta_N$ = 5.2 deg). Such subboundaries in the sigma phase can be the result of full transformation of ferrite (Fig. 19) and also can be introduced by the "ovulation processes" as suggested by Gill, *et al.* (Ref. 11). Figure 23 shows a sigma phase containing a grain boundary. Each of the sigma grains takes a near Nenno relationship with austenite, *i.e.*, ($\bar{1}$11) $\gamma$ // (00$\bar{1}$) $\sigma_1$ // (001) $\sigma_2$, [110] $\gamma$ // [110] $\sigma_1$, [0$\bar{1}$1] $\gamma$ // [$\bar{1}$10] $\sigma_2$. Since these orientation relationships are similar to the case of Fig. 20, the sigma transformation, as seen in Fig. 20, can lead to the sigma phase seen in Fig. 23. The sigma phase in Fig. 24 contains sub and grain boundaries, and each of the sigma grains does not take the Nenno relationship with austenite.

Although $M_{23}C_6$ was detected by x-ray diffractometry (Fig. 4), the amount was small, due to low carbon content. TEM observations of specimens heat treated for more than 86 ks showed only a few $M_{23}C_6$ grains at ferrite/austenite boundaries, and many of these had no $M_{23}C_6$. Therefore, the effect of $M_{23}C_6$ on sigma precipitation behavior may be very small in the present weld metal. Most of the $M_{23}C_6$ grains were observed at boundaries between vermicular ferrite and austenite. This suggests $M_{23}C_6$ may also be easy to precipitate at vermicular ferrite/austenite boundaries with low coherency. Each $M_{23}C_6$ grain took a parallel orientation to the contacted austenite, similarly to cases of precipitation at $\gamma/\gamma$ boundaries (Refs. 40–43).

In the present study, a large difference in sigma precipitation between lacy and vermicular ferrite structures were observed. If the initial (as-welded) ferrite structure can be controlled by welding conditions, methods or techniques without compositional changes, such as the cooling rate which can influence the ferrite composition between vermicular and lacy (Refs. 21, 44), it might be possible to retard the sigma precipitation to some extent at elevated temperatures.

## Conclusions

Delta-ferrite transformations and their crystallographic characteristics in a Type 304L austenitic stainless steel weld metal at elevated temperatures were observed mainly by transmission electron microscopy. The results are as follows:

1) Two types of ferrite morphologies, lacy and vermicular, coexist in the Type 304L steel weld metal. The lacy ferrite takes approximately the Kurdjumov-Sachs (K-S) relationship with austenite, but the vermicular one does not. Since the K-S relationship leads to a low-energy $\delta/\gamma$ boundary, the boundary coherency is higher in the lacy ferrite structure than in vermicular one. These crystallographic characteristics are maintained in each ferrite structure during heat treatments.

2) The ferrite transformation at 973 K is slower in the early stage, but becomes faster after being held a long time over 300 ks, when compared to 1073 K. This may be attributed to sigma formation at 973 K.

3) The heat treatment at 1073 K changes the ferrite shape, depending on the initial ferrite structure. The ferrite shape tends to become rectangular and long-slender with a directionality in the lacy structure, while roundish in the vermicular one.

4) Sigma precipitation at 973 K starts much earlier in the vermicular ferrite structure than in the lacy one. The larger the deviation angle of $\delta/\gamma$ from the K-S relationship, the easier is the sigma precipitation. The sigma phase takes several orientation relationships with austenite or ferrite.

5) The large differences in transformation behavior between lacy and vermicular ferrite structures can be explained by the $\delta/\gamma$ boundary coherency.

*Acknowledgments*

The authors wish to thank A. Honda and T. Koyanagawa for their help with the experiments. Financial support from the Japanese Ministry of Education, Science and Culture with a grant-in-aid for scientific research is gratefully acknowledged.

*References*

1. Hull, F. C. 1967. Effect of delta ferrite on the hot cracking of stainless steel. *Welding Journal* 46(9):399-s to 409-s.

2. Lundin, C. D., DeLong, W. T., and Spond, D. F. 1975. Ferrite-fissuring relationship in austenitic stainless steel weld metals. *Welding Journal* 54(8):241-s to 246-s.

3. Spruiell, J. E., Fett, W. E., and Lundin, C. D. 1977 Ferrite stability at elevated temperature in austenitic stainless steel weld metal. *Welding Journal* 56(9):289-s to 290-s.

4. David, S. A. 1981. Ferrite morphology and variations in ferrite content in austenitic stainless steel welds. *Welding Journal* 60(4):63-s to 71-s.

5. Lai, J. K., and Haigh, J. R. 1979. Delta-ferrite transformations in a Type 316 weld metal. *Welding Journal* 58(1):1-s to 6-s.

6. Keown, S. R., and Thomas, R. 1981. Role of delta ferrite in thermal aging of Type 316 weld metals. *Met. Sci.* 15(9):386-392.

7. Leitnaker, J. M. 1982. Prevention of chi and sigma phases formation in aged 16-8-2 weld metal. *Welding Journal* 61(1):9-s to 12-s.

8. Slattery, G. F., Keown, S. R., and Lambert, M. E. 1983. Influence of $\delta$-ferrite content on transformation to intermetallic phases in heat treated Type 316 austenitic stainless steel weld metal. *Met. Technol.* 10(10):373-385.

9. Vitek, J. M., and David, S. A. 1984. The solidification and aging behavior of Types 308 and 308CRE stainless steel welds. *Welding Journal* 63(8):246-s to 253-s.

10. Vitek, J. M., and David, S. A. 1986. The sigma phase transformation in austenitic stainless steels. *Welding Journal* 65(4):106-s to 111-s.

11. Gill, T. P. S., Vijayalakshmi, M., Gnanamoorthy, J. B., and Padmanabhan, K. A. 1986. Transformation of delta-ferrite during the postweld heat treatment of Type 316L stainless steel weld metal. *Welding Journal* 65(5):122-s to 128-s.

12. Farrar, R. A., and Thomas, R. G. 1983. The microstructure and phase transformations in duplex 316L submerged arc weld metals. *J. Mater. Sci.* 18:3461-3474.

13. Farrar, R. A. 1985. Microstructure and phase transformations in duplex 316 submerged arc weld metal—an aging study at 700°C. *J. Mater. Sci.* 20:4215-4231.

14. Takalo, T., Suutala, N., and Moisio, T. 1976. Influence of ferrite content on its morphology in some austenitic weld metals. *Met. Trans.* 7A (10):1591-1592.

15. Lippold, J. C., and Savage, W. F. 1979. Solidification of austenitic stainless steel weldments (Part I). *Welding Journal* 58(12):362-s to 374-s. *ibid.* 1980. (Part II), 59(2):48-s to 58-s.

16. Suutala, N., Takalo, T., and Moisio, T. 1979. The relationship between solidification and microstructure in austenitic and austenitic-ferritic stainless steel welds. *Met. Trans. A* 10A(4):512-514.

17. Takalo, T., Suutala, N., and Moisio, T. 1979. Austenitic solidification mode in austenitic stainless steel welds. *Met. Trans. A* 10A(8):1173-1181.

18. Suutala, N., Takalo, T., and Moisio, T. 1979. Single-phase ferritic solidification mode in austenitic-ferritic stainless steel welds. *Met. Trans. A* 10A(8):1183-1190.

19. Suutala, N., Takalo, T., and Moisio, T. 1980. Ferritic-austenitic solidification mode in austenitic stainless steel welds. *Met. Trans. A* 11A(5):717-725.

20. Suutala, N. 1982. Effect of manganese and nitrogen on the solidification mode in austenitic stainless steel welds. *Met. Trans. A* 13A(12):2121-2130.

21. Suutala, N. 1983. Effect of solidification conditions on the solidification mode in austenitic stainless steel welds. *Met. Trans. A* 14A(2):191-197.

22. Ritter, A. M., Cieslak, M. J., and Savage, W. F. 1983. Precipitation in CF-8M duplex stainless steel welds. *Met. Trans. A* 14A(1):37-44.

23. Kuwana, T., Kokawa, H., and Tsujii, H. 1986. The effect of the nitrogen absorption on the TEM structure of SUS 304L austenitic stainless steel weld metal. *Trans. Japan Weld. Soc.* 17(1):10-19.

24. Kurdjumov, G., and Sachs, G. 1930. *Z. Phys.* 64:325.

25. Kuwana, T., and Kokawa, H. 1985. Transmission electron microscope observations of SUS 304L austenitic stainless steel welds. *Trans. Japan Weld. Soc.* 16(2):99-109.

26. Okagawa, R. K., Dixon, R. D., and Olson, D. L. 1983. The influence of nitrogen from welding on stainless steel weld metal microstructures. *Welding Journal* 62(8):204-s to 209-s.

27. Warrington, D. H., and Bufalini, P. 1971. The coincidence-site lattice and grain boundaries. *Scripta Met.* 5(9):771-776.

28. Bollmann, W., Michaut, B., and Sainfort, G. 1972. Pseudo-subgrain-boundaries in stainless steel. *Phys. Stat. Sol.* (a) 13:637-649.

29. Grimmer, H., Bollmann, W., and Warrington, D. H. 1974. Coincidence-site lattices and complete pattern-shift lattices in cubic crystals. *Acta Cryst. A* 30:197-207.

30. Pumphrey, P. H. 1975. The use of transmission electron microscopy in the study of special high-angle grain boundaries in polycrystals. *Phys. Stat. Sol.* (a) 28:545-553.

31. Clark, W. A., and Smith, D. A. 1978. The dislocation structure of a $\Sigma = 9$ related coincidence boundary in stainless steel. *Phil. Mag. A* 38(4):367-385.

32. Tisinai, G. F., Stanley, J. K., and Samans, C. H. 1956. Sigma nucleation times in stainless steels. *J. Metals* 8(5):600-604.

33. Nenno, S., Tagaya, M., and Nishiyama, Z. 1962. Orientation relationships between gamma (f.c.c.) and sigma phases in an iron-chromium-nickel alloy. *Trans. JIM* 3:82-94.

34. Nenno, S., Tagaya, M., Hosomi, K., and Nishiyama, Z. 1963. Electron microscope study of sigma phase precipitation in an iron-chromium-nickel alloy. *Trans. JIM* 4:222-231.

35. Lewis, M. H. 1966. Precipitation of (Fe,Cr) sigma phase from austenite. *Acta Met.* 14(11):1421-1428.

36. Blenkinsop, P. A., and Nutting, J. 1967. Precipitation of the sigma phase in an austenitic steel. *JISI* 205(9):953-958.

37. Singhal, L. K., and Martin, J. W. 1968. The formation of ferrite and sigma-phase in some austenitic stainless steels. *Acta Met.* 16(12):1441-1451.

38. Beckitt, F. R., 1969. The formation of sigma phase from delta-ferrite in a stainless steel. *JISI* 207(5):632-638.

39. Shinohara, K., Seo, T., and Kumada, K. 1979. Recrystallization and sigma phase formation as concurrent and interacting phenomena in 25%Cr-20%Ni steel. *Trans. JIM* 20:713-723.

40. Lewis, M. H., and Hattersley. 1965. Precipitation of $M_{23}C_6$ in austenitic steels. *Acta Met.* 13(11):1159-1168.

41. Beckitt, F. R., and Clark, B. R. 1967. The shape and mechanism of formation of $M_{23}C_6$ carbide in austenite. *Acta Met.* 15(1):113-129.

42. Duhaj, P., Ivan, J., and Makovický, E. 1968. Sigma-phase precipitation in austenitic steels. *JISI* 206(12):1245-1251.

43. Pumphrey, P. H., and Edington, J. W. 1974. The structure of the semicoherent interface between grain boundary nucleated $M_{23}C_6$ and austenitic stainless steel. *Acta Met.* 22(1):89-94.

44. Kujanpää, V. P. 1984. Weld discontinuities in austenitic stainless steel sheets—effect of impurities and solidification mode. *Welding Journal* 63(12):369-s to 375-s.